# *In vivo* two-photon imaging of the mouse retina

**Robin Sharma,[1,2,*] Lu Yin,[1] Ying Geng,[1,2,6] William H. Merigan,[1,3] Grazyna Palczewska,[4] Krzysztof Palczewski,[5] David R. Williams,[1,2,3] and Jennifer J. Hunter[1,3]**

[1]*Center for Visual Science, University of Rochester, Rochester, New York 14627, USA*
[2]*The Institute of Optics, University of Rochester, Rochester, New York 14620, USA*
[3]*Flaum Eye Institute, University of Rochester, Rochester, New York 14642, USA*
[4]*Polgenix, Inc., 11000 Cedar Avenue, Suite 260, Cleveland, Ohio 44106, USA*
[5]*Department of Pharmacology, Case Western Reserve University, 10900 Euclid Avenue, Cleveland, Ohio 44106, USA*
[6]*Currently at: Corning Incorporated, One Riverfront Plaza, Corning, New York 14831, USA*
[*]*rsharma@optics.rochester.edu*

**Abstract:** Though *in vivo* two-photon imaging has been demonstrated in non-human primates, improvements in the signal-to-noise ratio (SNR) would greatly improve its scientific utility. In this study, extrinsic fluorophores, expressed in otherwise transparent retinal ganglion cells, were imaged in the living mouse eye using a two-photon fluorescence adaptive optics scanning laser ophthalmoscope. We recorded two orders of magnitude greater signal levels from extrinsically labeled cells relative to previous work done in two-photon autofluorescence imaging of primates. Features as small as single dendrites in various layers of the retina could be resolved and predictions are made about the feasibility of measuring functional response from cells. In the future, two-photon imaging in the intact eye may allow us to monitor the function of retinal cell classes with infrared light that minimally excites the visual response.

©2013 Optical Society of America

**OCIS codes:** (330.4460) Ophthalmic optics and devices; (180.4315) Nonlinear microscopy; (170.0110) Imaging systems.

## References and links

1. J. Liang, D. R. Williams, and D. T. Miller, "Supernormal vision and high-resolution retinal imaging through adaptive optics," J. Opt. Soc. Am. A **14**(11), 2884–2892 (1997).
2. A. Roorda, F. Romero-Borja, W. Donnelly Iii, H. Queener, T. Hebert, and M. Campbell, "Adaptive optics scanning laser ophthalmoscopy," Opt. Express **10**(9), 405–412 (2002).
3. D. C. Gray, W. Merigan, J. I. Wolfing, B. P. Gee, J. Porter, A. Dubra, T. H. Twietmeyer, K. Ahamd, R. Tumbar, F. Reinholz, and D. R. Williams, "*In vivo* fluorescence imaging of primate retinal ganglion cells and retinal pigment epithelial cells," Opt. Express **14**(16), 7144–7158 (2006).
4. Y. Geng, A. Dubra, L. Yin, W. H. Merigan, R. Sharma, R. T. Libby, and D. R. Williams, "Adaptive optics retinal imaging in the living mouse eye," Biomed. Opt. Express **3**(4), 715–734 (2012).
5. J. I. W. Morgan, A. Dubra, R. Wolfe, W. H. Merigan, and D. R. Williams, "*In vivo* autofluorescence imaging of the human and macaque retinal pigment epithelial cell mosaic," Invest. Ophthalmol. Vis. Sci. **50**(3), 1350–1359 (2008).
6. A. Dubra, Y. Sulai, J. L. Norris, R. F. Cooper, A. M. Dubis, D. R. Williams, and J. Carroll, "Noninvasive imaging of the human rod photoreceptor mosaic using a confocal adaptive optics scanning ophthalmoscope," Biomed. Opt. Express **2**(7), 1864–1876 (2011).
7. D. Scoles, D. C. Gray, J. J. Hunter, R. Wolfe, B. P. Gee, Y. Geng, B. D. Masella, R. T. Libby, S. Russell, D. R. Williams, and W. H. Merigan, "*In vivo* imaging of retinal nerve fiber layer vasculature: imaging histology comparison," BMC Ophthalmol. **9**(1), 1–9 (2009).
8. E. A. Rossi, M. Chung, A. Dubra, J. J. Hunter, W. H. Merigan, and D. R. Williams, "Imaging retinal mosaics in the living eye," Eye (Lond.) **25**(3), 301–308 (2011).
9. Y. Imanishi, M. L. Batten, D. W. Piston, W. Baehr, and K. Palczewski, "Noninvasive two-photon imaging reveals retinyl ester storage structures in the eye," J. Cell Biol. **164**(3), 373–383 (2004).
10. Y. Imanishi, K. H. Lodowski, and Y. Koutalos, "Two-photon microscopy: shedding light on the chemistry of vision," Biochemistry **46**(34), 9674–9684 (2007).

11. J. J. Hunter, B. Masella, A. Dubra, R. Sharma, L. Yin, W. H. Merigan, G. Palczewska, K. Palczewski, and D. R. Williams, "Images of photoreceptors in living primate eyes using adaptive optics two-photon ophthalmoscopy," Biomed. Opt. Express **2**(1), 139–148 (2010).

12. T. Euler, P. B. Detwiler, and W. Denk, "Directionally selective calcium signals in dendrites of starburst amacrine cells," Nature **418**(6900), 845–852 (2002).

13. L. Tian, S. A. Hires, T. Mao, D. Huber, M. E. Chiappe, S. H. Chalasani, L. Petreanu, J. Akerboom, S. A. McKinney, E. R. Schreiter, C. I. Bargmann, V. Jayaraman, K. Svoboda, and L. L. Looger, "Imaging neural activity in worms, flies, and mice with improved GCaMP calcium indicators," Nat. Methods **6**(12), 875–881 (2009).

14. K. Ohki, S. Chung, Y. H. Ch'ng, P. Kara, and R. C. Reid, "Functional imaging with cellular resolution reveals precise micro-architecture in visual cortex," Nature **433**(7026), 597–603 (2005).

15. L. Yin, Y. Geng, F. Osakada, R. Sharma, A. H. Cetin, E. M. Callaway, D. R. Williams, and W. H. Merigan, "Imaging light responses of retinal ganglion cells in the living mouse eye," J. Neurophysiol. **109**(9), 2415–2421 (2013).

16. A. Dubra and Z. Harvey, "Registration of 2D Images from Fast Scanning Ophthalmic Instruments," in *Biomedical Image Registration*, Lecture Notes in Computer Science, B. Fischer, B. Dawant, and C. Lorenz, eds. (Springer Berlin / Heidelberg, 2010), **6204**, 60–71.

17. J. T. Dobbins III, "Image quality metrics for digital system," in *Handbook of Medical Imaging, Volume 1. Physics and Psychophysics*, R. L. Van Metter, J. Beutel, and H. L. Kundel, eds. (SPIE, 2000).

18. L. Yin, K. Greenberg, J. J. Hunter, D. Dalkara, K. D. Kolstad, B. D. Masella, R. Wolfe, M. Visel, D. Stone, R. T. Libby, D. Diloreto, Jr., D. Schaffer, J. Flannery, D. R. Williams, and W. H. Merigan, "Intravitreal injection of AAV2 transduces macaque inner retina," Invest. Ophthalmol. Vis. Sci. **52**(5), 2775–2783 (2011).

19. F. Osakada, T. Mori, A. H. Cetin, J. H. Marshel, B. Virgen, and E. M. Callaway, "New rabies virus variants for monitoring and manipulating activity and gene expression in defined neural circuits," Neuron **71**(4), 617–631 (2011).

20. W. Wei, J. Elstrott, and M. B. Feller, "Two-photon targeted recording of GFP-expressing neurons for light responses and live-cell imaging in the mouse retina," Nat. Protoc. **5**(7), 1347–1352 (2010).

21. M. Pottek, G. C. Knop, R. Weiler, and K. Dedek, "Electrophysiological characterization of GFP-expressing cell populations in the intact retina," J. Vis. Exp. (57), 13473–13474 (2011).

22. B. G. Borghuis, L. Tian, Y. Xu, S. S. Nikonov, N. Vardi, B. V. Zemelman, and L. L. Looger, "Imaging light responses of targeted neuron populations in the rodent retina," J. Neurosci. **31**(8), 2855–2867 (2011).

23. J. Coombs, D. van der List, G.-Y. Wang, and L. M. Chalupa, "Morphological properties of mouse retinal ganglion cells," Neuroscience **140**(1), 123–136 (2006).

24. F. Naarendorp, T. M. Esdaille, S. M. Banden, S. Andrews-Labenski, O. P. Gross, and E. N. Pugh, Jr., "Dark light, rod saturation, and the absolute and incremental sensitivity of mouse cone vision," J. Neurosci. **30**(37), 12495–12507 (2010).

25. Y. V. Wang, M. Weick, and J. B. Demb, "Spectral and temporal sensitivity of cone-mediated responses in mouse retinal ganglion cells," J. Neurosci. **31**(21), 7670–7681 (2011).

26. T. D. Lamb, "Photoreceptor spectral sensitivities: common shape in the long-wavelength region," Vision Res. **35**(22), 3083–3091 (1995).

27. E. J. Gualda, J. M. Bueno, and P. Artal, "Wavefront optimized nonlinear microscopy of *ex vivo* human retinas," J. Biomed. Opt. **15**(2), 026007 (2010).

28. R.-W. Lu, Y.-C. Li, T. Ye, C. Strang, K. Keyser, C. A. Curcio, and X.-C. Yao, "Two-photon excited autofluorescence imaging of freshly isolated frog retinas," Biomed. Opt. Express **2**(6), 1494–1503 (2011).

## 1. Introduction

Adaptive optics scanning laser ophthalmoscopy (AOSLO) permits diffraction-limited imaging of microscopic structures in the human, primate and mouse retinas [1–4]. Thanks to advances in system design and image registration software, imaging of many different cell classes in the retina is now possible in reflectance and single-photon fluorescence imaging modes [5–8]. Two-photon fluorescence imaging has the potential for imaging both intrinsic and extrinsic fluorophores in the retina using infrared light [9,10]. With the aid of adaptive optics, two-photon retinal imaging through the pupil has been demonstrated in the living primate [11]. However, despite the high light levels used, signal levels were far too low for practical scientific investigations requiring long imaging and integration times. This precludes the ability to image cellular functional responses. Thus, it is necessary to improve signal levels to decrease required imaging times and make two-photon fluorescence imaging practical. In this work, we took two approaches to improve fluorescence; shifting from monkey to mouse, and using extrinsic fluorophores that have greater fluorescence cross-sections than intrinsic fluorophores. The mouse has been shown to be a better model for retinal imaging due to the higher numerical aperture of the eye and the ability to resolve smaller structures [4].

Furthermore, availability of a variety of transgenic and retinal disease models, as well as the relative ease with which cells can be labeled, makes the mouse a desirable species for developing functional imaging tools. The goal of this paper is to demonstrate that the combination of these approaches enhances the utility of two-photon imaging as a practical functional imaging tool for scientific studies in the living eye.

It is now possible to label specific cell classes with fluorophores such as calcium indicators, the fluorescence intensity of which changes with cell activation [12–14]. Functional activation of ganglion cells labeled with a genetically encoded calcium indicator, G-CaMP3, has previously been recorded with an AOSLO in mouse eyes by Yin et al *in vivo* using conventional single-photon excitation methods [15]. We have applied two-photon imaging to visualize retinal ganglion cells labeled with green fluorescent protein (GFP) and G-CaMP3 and ascertained the feasibility and prospective accessibility of cell activation studies in the neural circuitry in the living mouse eye.
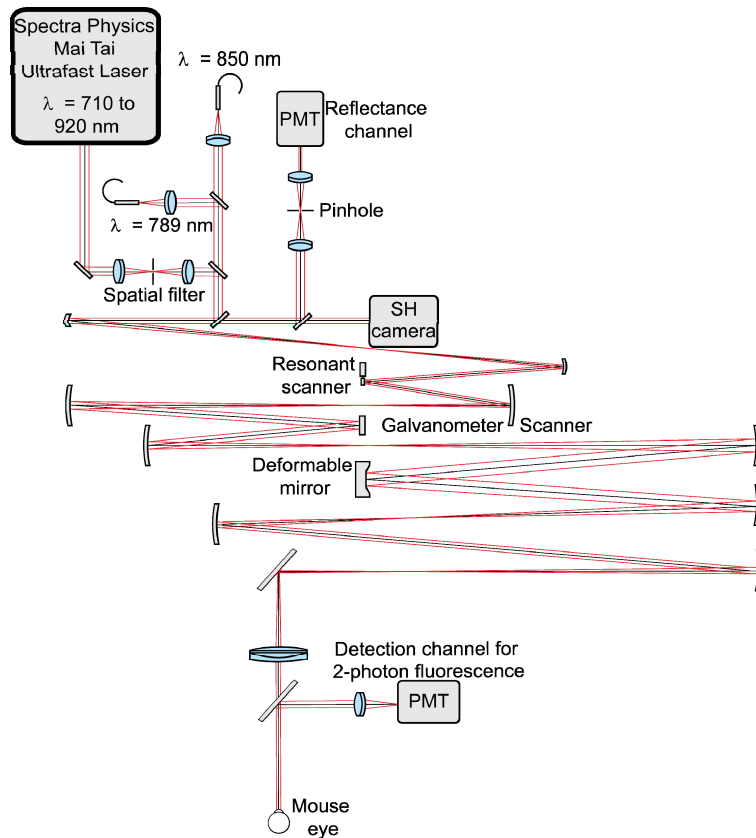


Fig. 1. Layout of 2PAOSLO for imaging mouse retina. Light from the pulsed ultrafast laser passes through the DeepSee dispersion compensation attachment (not shown) and is then focused through a spatial filter to generate a point source of light. The detection channel for two-photon fluorescence collection as shown in the diagram is close to the eye and fluorescence emitted by cells in the eye is directed into this detector using a dichroic that reflects visible light and transmits infrared wavelengths. For reflectance imaging and wavefront sensing, light scattered from the retina propagates back through the system and is detected near the light sources, as is typical in most AOSLO systems. The rest of the system is identical to the AOSLO described previously by Geng et al [4].

## 2. Methods

### 2.1 System

A previously described AOSLO for imaging the mouse eye [4] was modified to permit two-photon imaging (Fig. 1). A laser diode at 850 nm (QPhotonics, Ann Arbor, Michigan, USA) was used for wavefront sensing and a superluminescent diode at 789 nm (SLD, InPhenix, Livermore, California, USA) was employed for reflectance imaging. A pulsed laser (Mai Tai XF-1, Newport Spectra-Physics, Santa Clara, CA, USA) operating at a pulse repetition rate of 80 MHz was used for exciting two-photon fluorescence. Light from the free-space, ultrafast laser was focused through a spatial filter so as to generate a point source and then, with a collimating achromatic doublet lens was coupled into the entrance pupil of the AOSLO system. The other light sources were fiber-coupled and also routed into the AOSLO. The three light sources were focused at different layers in the retina; the wavefront sensor was focused at the outer retina, the SLD was focused at vascular structure in the inner retina and the two-photon excitation source was focused at the ganglion cell layer. To achieve this, the wavefront curvature of each light source was independently adjusted at the entrance pupil of the system.

During an experiment, the deformable mirror (DM97, ALPAO SAS, Grenoble, France) provided enough stroke to correct aberrations of the eye and also change the depths at which all light sources focused. A lenslet array (Adaptive Optics Associates, Cambridge, Massachusetts, USA), placed in front of a CCD camera (Rolera XR, QImaging, Surrey, British Columbia, Canada), was used for wavefront sensing. A photomultiplier tube (PMT H7422-40, Hamamatsu Corporation, Shizuoka-Ken, Japan) was used for reflectance imaging through a confocal pinhole of aperture size 4.8 Airy discs (50 μm).

The pulsed laser emits ultrashort pulses of width < 70 fs and the central wavelength can be tuned from 710 nm to 920 nm. For two-photon fluorescence from GFP and G-CaMP3 labeled ganglion cells, the laser was operated at a central wavelength of 920 nm and full width half maximum (FWHM) spectral bandwidth of about 18 nm. At this wavelength, the power of the excitation source at the pupil of the eye was 9.5 mW for the GFP imaging experiments and 6 mW for the G-CaMP3 experiments. Dispersion was compensated through use of a pair of prisms placed on motorized stages within the DeepSee attachment of the Mai Tai XF-1 laser.

The two-photon AOSLO (or 2PAOSLO) has intrinsic axial sectioning capabilities and therefore the emitted fluorescence was not de-scanned and a pinhole was not required for confocal detection. All fluorescence in the visible spectrum emitted back through the pupil of the eye is directly diverted to a separate detection channel with a dichroic mirror (FF665-Di02, Semrock, Rochester, NY, USA). A collector lens was used to direct emitted fluorescence into a photomultiplier tube (PMT H7422-40, Hamamatsu Corporation, Japan) placed in a plane conjugate to the pupil of the eye. Two filters (ET680SP-2P8, Chroma Technology Corporation, Bellows Falls, Vermont, USA) were used to avoid bleed-through of backscattered excitation light. The optical density (OD) of each filter was greater than 6.5 at wavelengths above 720 nm. Since a confocal pinhole is not used, the detector was much more sensitive to stray light than conventional AOSLO systems. Hence, the system was baffled completely to prevent stray room-light from reaching the PMT and a black sheet was used to cover the system and the animal. The noise floor and the SNR were dominated by background stray light and were therefore improved by its suppression. We quantified the noise floor in the detection channel to be less than 5-10% of the two-photon signal from GFP labeled cells.

### 2.2 Image acquisition and analysis

Images were acquired at a frame rate of 22 Hz, slower than previous experiments with mouse imaging [4,15]. Due to the breathing motion of the anesthetized animal, there was noticeable motion in the image collected from one frame to the next. The two-photon fluorescence signal was too weak to enable accurate estimation of the motion from frame to frame, so we

simultaneously collected a high contrast reflectance video of vascular structures in the inner retina. The contrast due to the vessels provided the post-processing registration signal from which eye motion could be corrected. Once fluorescent cells were identified, videos from each location were recorded at different axial depths by changing the curvature of the wavefront with the deformable mirror. The protocol for image acquisition and registration was described in detail previously [4,11,16]. ImageJ (NIH, Maryland, USA) was used to perform an analysis of mean gray levels in single cells as well as clusters of cells. For estimating mean gray levels, stabilized 8-bit videos were loaded into ImageJ and cells were encircled. The region of interest (ROI) manager plugin was utilized to measure the average signal levels within the encircled cell area for each frame of the video. Calculations of photons collected per pixel were estimated from the mean gray levels reported by the detection channel for known incident power values at the same PMT gain and the SNR was then estimated by using Poisson statistics [17].

### 2.3 Animal preparation

Black C57BL/6J mice from 2 to 21 months of age were used in this study. All experiments were approved by the University Committee on Animal Resources at the University of Rochester. For an initial demonstration of two-photon imaging in the intact eye of the living mouse, GFP was used for labeling cells in the retina because it is a highly efficient fluorophore and the labeling techniques are well established.
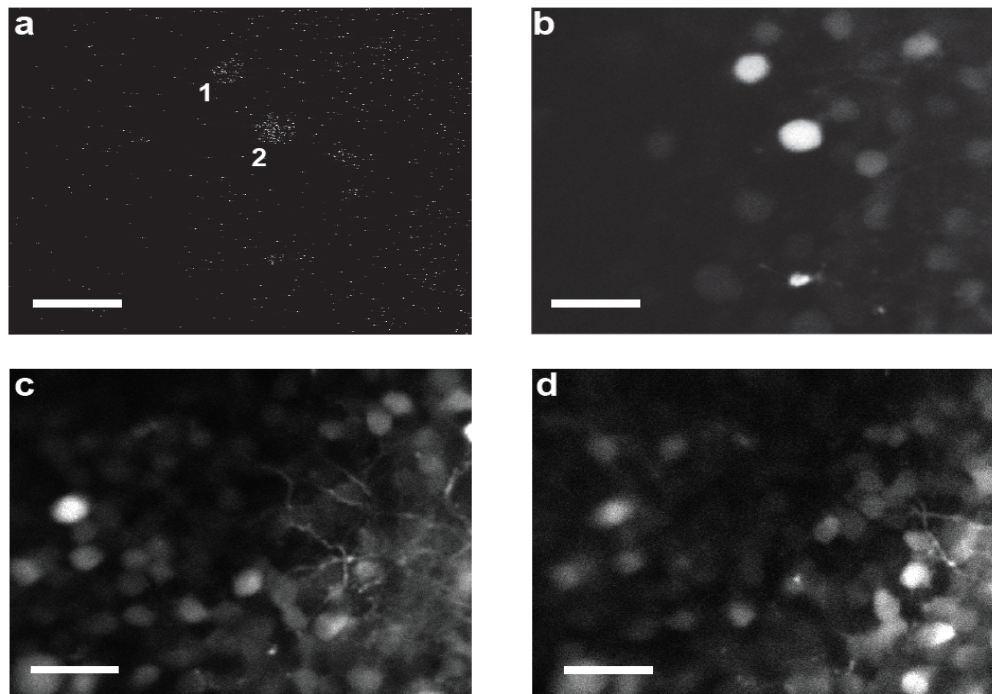


Fig. 2. Images of GFP labeled cells. Panel (a) is a single frame taken from a video showing the real-time two-photon signal from labeled ganglion cells (Media 1). Panel (b) is a registered image of 5000 frames of the video in panel (a). Two bright cells are visible (labeled 1 and 2 in (a)) as well as many additional fainter cells that are likely at different depths. Panels (c) and (d) show inner retinal cells at the same retinal location but at axial depths separated by 5 μm. Subcellular structures, including dendritic morphology are clearly visible. This shows that the system has sufficient intrinsic axial sectioning capabilities despite the absence of a confocal pinhole. Scale bar is 50 μm. Images are contrast stretched for optimal visualization.

A subset of mice was injected intravitreally with adeno-associated viral (AAV) vector, serotype 2, carrying GFP gene driven by human connexin 36 (hCx36) promoter [18] (produced in the laboratory of Dr. John G. Flannery, Helen Wills Neuroscience Institute, University of California, Berkeley, CA, USA) to target cells of the inner retina, including ganglion and amacrine cells. The distribution of labeled cells in the retina was verified post-injection by low resolution fundus imaging (HRA Spectralis Gmbh, Heidelberg, Germany). A separate group of mice received retrograde injections of rabies viral vector, carrying G-CaMP3 and DsRed genes (produced in the laboratory of Dr. Edward M. Callaway, Salk Institute for Biological Study, San Diego, CA, USA). Injections were made into the superior colliculus, a retino-recipient nucleus [15,19] labeling ganglion cells through retrograde transport. For *in vivo* imaging, mice were anesthetized with Ketamine/Xylazine cocktail injections. After the injections, their pupils were dilated with a drop each of tropicamide and phenylephrine (Neo-Synephrine) and then placed in a bite-bar mount with a heating pad and anesthetized further under isofluorane gas. Details of this imaging protocol have been described in entirety in an earlier publication [4].

## 3. Results

### 3.1 Two-photon imaging of GFP-labeled inner retinal cells

Cell somas were most clearly labeled and were the easiest structure of ganglion cells to identify. The mean signal level was of the order of 0.02 photons per pixel per cell soma. We confirmed that fluorescent signals were consistent with the properties of non-linear fluorescence because optimizing the dispersion compensation applied by the DeepSee module provided enhanced signal collection. All subsequent imaging was performed after optimizing this setting. Fluorescence intensity across individual cell somas was higher than dendrites and in many cases it was possible to identify cell somas in a single frame during real time imaging (Media 1). Additional soma and dendrites were only visible after off-line registration. Different cellular features could be identified in different planes by changing the depth at which the incident beam was focused. Although the axial resolution of the system has not been thoroughly quantified, differences in dendritic morphology can be visually identified from videos recorded at the same retinal location, but at planes differing in axial depth by only 5 μm [Fig. 2 (c) and 2(d)].



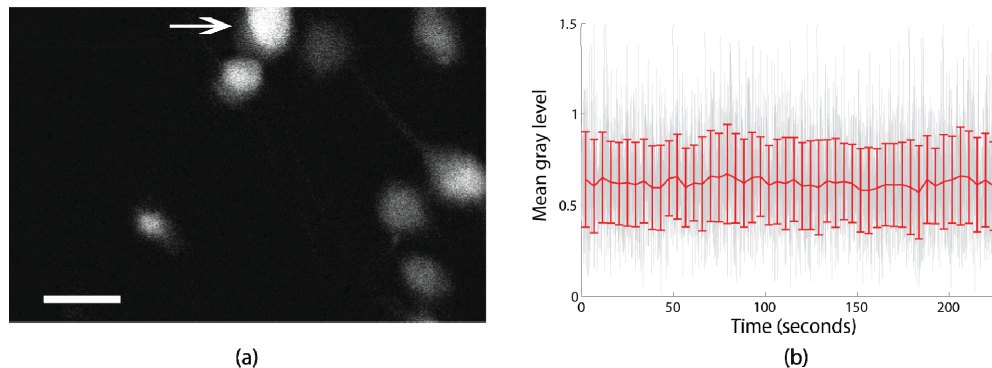(a)                                    (b)

Fig. 3. (a) Image of ganglion cells labeled with calcium indicator G-CaMP3. Arrow in white points to the cell that was used for analysis of SNR of *in vivo* two-photon fluorescence imaging of G-CaMP3 labeled cells (outlined detail in the discussion section), (b) Plot of the signal level from the cell marked with the white arrow in the image shown in (a) over time showing stable activation and minimal photobleaching. The raw data for each frame has been plotted in gray. The mean gray level averaged over every 1 second has been plotted in red. Error bars represent the standard deviation of the mean. Scale bar shown in (a) is 50 μm. Image is contrast-stretched for display purposes.

*3.2 Two-photon imaging of G-CaMP3 labeled ganglion cells*

Although the fluorescence efficiency of G-CaMP3 is lower than that of GFP [10], registered videos revealed many ganglion cell somas across the imaged field of view [Fig. 3(a)]. The mean signal collected from individual cell somas was on the order of 0.003 photons per pixel, one order of magnitude above the noise floor of the system. Even at the light levels used, the signal from individual cell somas remained stable with a standard deviation of 0.44 for the mean gray level [Fig. 3(b)]. At different focus depths some axons [Fig. 3(a)] and dendrites were visible, but not well defined.

## 4. Discussion and conclusions

Previously, *in vitro* two-photon microscopy has been used as a tool for imaging GFP-labeled cells in the mouse retina for morphological characterization of different cell classes. This was done in conjunction with electrophysiology and patch-clamp methods for recording functional signals from the retina [20,21]. Recently, *in vitro* two-photon imaging of neurons labeled with G-CaMP3 has also been demonstrated [22], which offers the possibility of simultaneously recording functional responses from many cells. Our work is the first to demonstrate two-photon imaging of GFP and G-CaMP3 labeled cells in an intact and living mouse through the pupil of the eye. We show here that the axial and lateral resolutions are sufficient to resolve many important structural features of ganglion cells, such as somas, axons and dendrites. The axial sectioning makes it possible to resolve dendritic features in different layers separated by 5 μm. *In vitro* preparations generally limit functional recording to a few hours, but *in vivo* imaging has the potential to track cellular function over weeks, months, and possibly even years.

The signal levels obtained from intrinsic fluorophores during previous *in vivo* two-photon imaging efforts in primate retina were prohibitively low and required excessively high signal integration times to generate images with adequate contrast [11]. The labeling and imaging protocol here provided sufficient two-photon fluorescence signal to enable visualization of single cells in real time in the mouse eye. Depending on the cell, the signal was at least one to two orders of magnitude greater than the noise floor. Residual noise in the system was due to a combination of photon noise, electronic noise, and stray light. Higher fluorescence signal levels enabled the operators to locate labeled cells easily and thus image a greater number of cells in less time. Furthermore, after registration and averaging, many more cells can be seen than what could be seen in real time. These improvements in signal levels can be attributed to the stronger quantum efficiency of the extrinsic fluorophores deployed as opposed to the intrinsic fluorophores imaged in the primate retina and also to the larger numerical aperture of the mouse eye [4].

From measurements of the total noise in our optical recordings, we can estimate the amount of signal averaging over space and time required to detect a given change in the fluorescence signal produced by visual stimulation. We define the sensitivity of our functional imaging system as the smallest change in the fluorescence signal that is distinguishable from the baseline fluorescence, which is inversely proportional to the SNR. In the inevitable presence of noise, one can increase the SNR through spatial (i.e. binning pixels), and/or temporal (i.e. averaging frames) integration. There are practical limits on the amount of spatial and temporal integration possible set by the size of the retinal feature one wishes to record from and the rate at which the optical response changes over time. The average SNR of all the pixels corresponding to the soma of a single ganglion cell labeled with G-CaMP3, shown in Fig. 3(a), is 0.06. Treating this number as typical of our current imaging capability, we can calculate the amount of spatial and/or temporal integration required to achieve a desired SNR (similar to Dobbins [17]), as shown in Fig. 4. For example, for soma area of 600 $\mu m^2$, a 1% change in fluorescence could be detected in 60 seconds using an instrument running at 25 Hz frame rate (to be used in future implementations of two-photon imaging) and

35 MHz pixel clock. This corresponds to a total dwell time of 0.12 seconds for the cell soma. This is achievable in one stable imaging session, or multiple imaging sessions could be combined if needed. Thus, our current light levels and experimental paradigms do permit *in vivo* functional measurements with two-photon imaging. However, because the efficacy of transduction of GFP and G-CaMP3 is not the same for all cells in the retina, the required duration of imaging for each cell might differ, depending also on many other factors such as the adaptive optics correction applied, PMT gain settings and light levels used.

In comparison, a typical SNR for single-photon imaging of GCaMP3 is 3.6 times greater than that of two-photon for light levels used by Yin et al [15]. For the example given above, only 3 seconds would be required in single-photon imaging to detect a 1% fluorescence change.
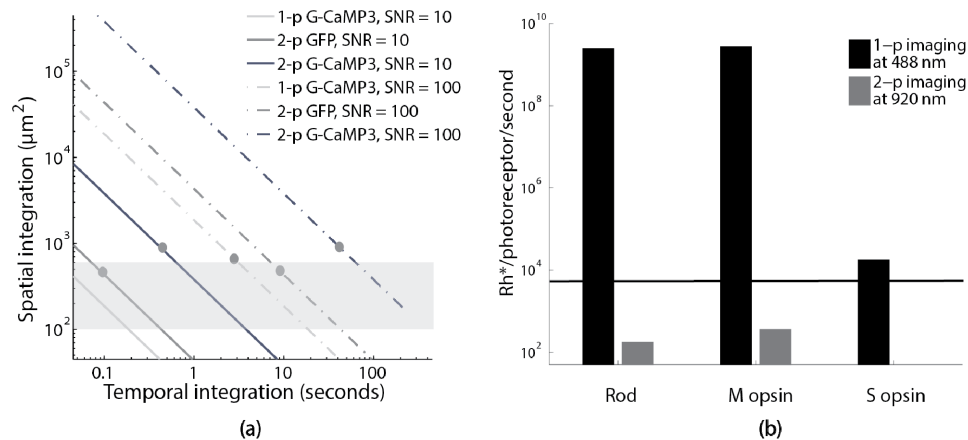


Fig. 4. (a) Plot of spatio-temporal integration required to capture sufficient signal (SNR ~10 and ~100) from individual ganglion cells labeled with GFP and G-CaMP3 when imaged with single-photon or two-photon imaging modalities. The figure shows a trade-off between spatial and temporal integration for collecting fluorescence signals at equal SNRs. The solid gray dots represent data points from *in vivo* imaging experiments. Single-photon G-CaMP3 data is from Yin et al [15]. The shaded region between the two dashed horizontal lines indicates the range of cell sizes for ganglion cells from literature [23] (b) Comparison of visual pigment isomerization in the mouse retina between single-photon imaging using 200 μW of 488 nm light and two-photon imaging using 6 mW of 920 nm light for imaging of G-CaMP3 labeled ganglion cells. The black horizontal line corresponds to the commencement of the photopic regime for the mouse visual system (5200 Rh*/photoreceptor/sec) [24–26].

Despite the fact that single-photon imaging produces a higher SNR than two-photon imaging, there remains a distinct spectral advantage of two-photon imaging because infrared wavelengths are far less likely to excite photoreceptor visual pigments. Light at 488 nm is close to the peak of spectral sensitivities of the rhodopsin and middle-wavelength sensitive (M) cone pigments in the mouse photoreceptors [24,25]. There is little experimental data on spectral sensitivity measurements in the mouse retina at 920 nm; however, previous studies have indicated that in other mammalian retina photopigment sensitivities decline linearly at long wavelengths beyond the visible spectrum [26]. This same trend would be expected in the mouse and an extrapolation of known spectral sensitivity data has been used to calculate visual pigment excitation using 488 nm at 200 μW for single-photon imaging and with 920 nm light at 6 mW for two-photon imaging. Figure 4(b) shows that despite the higher light levels used, the rhodopsin and M-opsin in the mouse retina are more than 6 orders of magnitude less sensitive for two-photon compared to single-photon excitation. The S-opsin is not at all sensitive to 920 nm light.

The reduced risk of photochemical damage to the retina is another advantage of using near-infrared wavelengths, however, the potential for thermal damage still exists. The safety

limits for mouse imaging can be inferred from the ANSI maximum permissible exposure for humans by equating the photon density at the retina. This provides a scaling factor for the MPE which is equal to the square of the ratio of the numerical apertures of human (0.24) and mouse (0.49) eyes. As a result, the light levels that were used for two-photon imaging of GFP and G-CaMP3 labeled cells were, respectively, factors of 12 and 7.5 times greater than the scaled safety limits. Despite this, low-resolution fundus imaging did not reveal any noticeable damage in the retinal tissue at the imaged locations, possibly because the assumption of equivalent molecular composition of mouse and human retinas may be invalid. Therefore, initial findings suggest that safe two-photon imaging in rodents is feasible.

With the improvements discussed here, *in vivo* two-photon retinal imaging in mouse will permit structural and functional imaging experiments employing spatio-temporal patterns to identify new visual system pathways. Further, it has the potential to pave the way for truly non-invasive *in situ* functional imaging of endogenous fluorescence [9,27,28] from all retinal cell classes in the living eye.

## Acknowledgments